

Hidden-charm tetraquarks with strangeness in the chiral quark model

Gang Yang,^{1,*} Jialun Ping,^{2,†} and Jorge Segovia^{3,‡}

¹*Department of Physics, Zhejiang Normal University, Jinhua 321004, China*

²*Department of Physics and Jiangsu Key Laboratory for Numerical Simulation of Large Scale Complex Systems, Nanjing Normal University, Nanjing 210023, P. R. China*

³*Departamento de Sistemas Físicos, Químicos y Naturales, Universidad Pablo de Olavide, E-41013 Sevilla, Spain*

The hidden-charm tetraquarks with strangeness, $c\bar{c}s\bar{q}$ ($q = u, d$), in $J^P = 0^+, 1^+$ and 2^+ are systematically investigated in the framework of real- and complex-scaling range of a chiral quark model, whose parameters have been fixed in advance describing hadron, hadron-hadron and multi-quark phenomenology. Each tetraquark configuration, compatible with the quantum numbers studied, is taken into account; this includes meson-meson, diquark-antidiquark and K-type arrangements of quarks with all possible color wave functions in four-body sector. Among the different numerical techniques to solve the Schrödinger-like 4-body bound state equation, we use a variational method in which the trial wave function is expanded in complex-range Gaussian basis functions, which is characterized by its simplicity and flexibility. This theoretical framework has already been used to study different kinds of multi-quark systems, such as the hidden-charm pentaquarks, P_c^+ , and doubly-charmed tetraquarks, T_{cc}^+ . The recently reported Z_{cs} states by the BESIII and LHCb collaborations are generally compatible with either compact tetraquark or hadronic molecular resonance configurations in our investigation. Moreover, several additional exotic resonances are found in the mass range between 3.8 GeV and 4.6 GeV.

I. INTRODUCTION

A structure with a significance of 5.3σ was reported in the process of $e^+e^- \rightarrow K^+(D_s^- D^{*0} + D_s^{*-} D^0)$ by the BESIII collaboration [1], its experimentally measured mass and width were $3982.5^{+1.8}_{-2.6} \pm 2.1$ MeV and $12.8^{+5.3}_{-4.4} \pm 3.0$ MeV, respectively. Undoubtedly, the named $Z_{cs}(3985)$ state was the first candidate of a charged hidden-charm tetraquark state with strangeness.

Later on, more charmonium-like states with strange content were reported by the LHCb collaboration in proton-proton collisions [2]. The $Z_{cs}(4000)$ is observed in the $B^+ \rightarrow J/\psi\phi K^+$ decay, with mass and width $4003 \pm 6^{+4}_{-14}$ MeV and $131 \pm 15 \pm 26$ MeV, and the preferred spin-parity is $J^P = 1^+$. The $X(4685)$, also with $J^P = 1^+$ quantum numbers, decays to $J/\psi\phi$ final state with a high significance claimed by the collaboration. Furthermore, the $Z_{cs}(4220)$ and $X(4630)$ are also reported with significance exceeding 5σ derivations. These facts trigger many theoretical investigations on the nature of hidden-charm tetraquark with strangeness.

In many theoretical works the $Z_{cs}(3985)$ is identified as the strange partner of the $Z_c(3900)$ within the $SU(3)_f$ symmetry, and thus the hadronic molecular configuration is proposed. In particular, the $D^*\bar{D}_s - D\bar{D}_s^*$ and $D^*\bar{D}_s^*$ molecules with spin-parity $J^P = 1^+$ state can be related to the mentioned $Z_{cs}^{(*)}$ particles [3]. This result is also supported by a coupled-channel calculation [4], a variety of effective field theory frameworks [5–8], approaches based on QCD sum rules [9, 10] and potential

model descriptions [11]. Finally, within the framework of an effective range expansion, a unified description of the hidden-charm tetraquark states $Z_c(3900)$, $Z_{cs}(3985)$ and $X(4020)$ are discussed [12]. Meanwhile, the 2- and 4-body configuration mixing scheme for describing the $Z_{cs}(3985)$ state has been proposed to be crucial in many theoretical investigations, *viz.* the $Z_{cs}(3985)$ is excluded as a pure $D^{*0}D_s^-/D^0D_s^{*-}/D^{*0}D_s^{*-}$ hadronic molecular state in, for instance, one-boson-exchange model [13, 14] and constituent quark model [15]. The $Z_{cs}(3985)$ and $Z_{cs}(4003)$ can be explained well within a mixture formalism in Refs. [16, 17].

Notwithstanding this, many theoretical approaches conclude that a compact tetraquark structure is also possible for the $Z_{cs}(3985)$, *e.g.* one-boson-exchange model [14], constituent quark model [15] and QCD sum rules [18]. Furthermore, some novel pictures for the $Z_{cs}(3985)$ state are proposed. Particularly, the $Z_{cs}(3985)$ can be identified as a reflection structure of charmed-strange meson $D_{s2}^*(2573)$ [19]. It is also explained as a genuine state, either virtual or bound, in a contact potential model [20]. Additionally, the photo-production [21] and properties of $Z_{cs}(3985)$ in hot dense medium [22, 23] have been recently studied theoretically.

Concerning the $Z_{cs}(4000)$, $Z_{cs}(4220)$, $X(4630)$ and $X(4685)$ states, there are in the literature interpretations compatible with hadronic molecules [24–27], compact tetraquark structures [27–30] and even non-resonance configurations [31]. Besides, the magnetic moments of the $Z_{cs}(4000)$ and $Z_{cs}(4220)$ are calculated by means of light-cone QCD sum rules [32].

In order to disentangle the nature of these charmonium-like resonances with strangeness announced recently by the LHCb and BESIII collaborations, a systematical investigation on the hidden-charm tetraquarks

* yanggang@zjnu.edu.cn

† jlping@njnu.edu.cn

‡ jsegovia@upo.es

with strange content: $c\bar{c}s\bar{q}$ ($q = u, d$), is performed within a chiral quark model formalism. The same theoretical framework has already been applied with success in the description of other multi-quark systems, *e.g.*, hidden-charm and -bottom pentaquarks [33, 34], doubly-charm pentaquarks [35], doubly-heavy tetraquarks, $QQ\bar{q}\bar{q}$ [36, 37] and strange-heavy tetraquarks, $sQ\bar{q}\bar{q}$ ($q = u, d, s; Q = c, b$) [38]. Particularly, we have explained the hidden-charm pentaquarks [33], $P_c^+(4312)$, $P_c^+(4380)$, $P_c^+(4440)$ and $P_c^+(4457)$, reported by the LHCb collaboration [39, 40], and predicted the doubly charmed tetraquark [36], T_{cc}^+ , announced very recently by the same experimental collaboration [41, 42]. It is also worth highlighting that the same theoretical approach was previously applied to the charmonium, bottomonium and heavy baryon sectors, studying their spectra [43–46], their electromagnetic, weak and strong decays and reactions [47–50], and their coupling with meson-meson thresholds [51–54].

Our formulation in real- and complex-scaling method of the theoretical formalism has been discussed in detail in Ref. [55]. The complex-scaling method (CSM) allows us to distinguish three kinds of scattering singularities: bound, resonance and scattering; which allows us to perform a complete analysis of the scattering problem within the same formalism. Furthermore, the meson-meson, diquark-antidiquark and K-type configurations, plus their couplings, are considered for the tetraquark system. Finally, the Rayleigh-Ritz variational method is employed in dealing with the spatial wave functions of the $c\bar{c}s\bar{q}$ tetraquark states, which are expanded by means of the well-known Gaussian expansion method (GEM) of Ref. [56].

The manuscript is arranged as follows. In Sec. II the theoretical framework is presented; we briefly describe the complex-range method applied to a chiral quark model and the $c\bar{c}s\bar{q}$ ($q = u, d$) tetraquark wave-functions. Section III is devoted to the analysis and discussion of the obtained low-lying $c\bar{c}s\bar{q}$ ($q = u, d$) tetraquark states with $J^P = 0^+, 1^+$ and 2^+ , and isospin $I = 1/2$. Finally, we summarize and give some prospects in Sec. IV.

II. THEORETICAL FRAMEWORK

A throughout review of the theoretical formalism used herein has been recently published in Ref. [55]. We shall, however, focus on the most relevant features of the chiral quark model and the numerical method concerning the strange hidden-charm tetraquarks, *viz.* the $c\bar{c}s\bar{q}$ system.

Within the so-called complex-range investigations, the relative coordinate of a two-body interaction is rotated in the complex plane by an angle θ , *i.e.* $\vec{r}_{ij} \rightarrow \vec{r}_{ij}e^{i\theta}$. Therefore, the general form of the four-body Hamiltonian

reads:

$$H(\theta) = \sum_{i=1}^4 \left(m_i + \frac{\vec{p}_i^2}{2m_i} \right) - T_{\text{CM}} + \sum_{j>i=1}^4 V(\vec{r}_{ij}e^{i\theta}), \quad (1)$$

where m_i is the quark mass, \vec{p}_i is the quark's momentum, and T_{CM} is the center-of-mass kinetic energy. According to the so-called ABC theorem [57, 58], the complex scaled Schrödinger equation:

$$[H(\theta) - E(\theta)] \Psi_{JM}(\theta) = 0 \quad (2)$$

has (complex) eigenvalues which can be classified into three different kinds: bound, resonance and continuum (scattering) states. Those which are either bound or resonance are independent of the rotated angle θ ; however, the first ones are always fixed on the coordinate-axis (there is no imaginary part of the eigenvalue), whereas the second ones are located above the corresponding threshold lines with a total decay width $\Gamma = -2\text{Im}(E)$.

The dynamics of the $c\bar{c}s\bar{q}$ tetraquark system is driven by a two-body potential

$$V(\vec{r}_{ij}) = V_\chi(\vec{r}_{ij}) + V_{\text{CON}}(\vec{r}_{ij}) + V_{\text{OGE}}(\vec{r}_{ij}), \quad (3)$$

which takes into account the most relevant features of QCD at its low energy regime: dynamical chiral symmetry breaking, confinement and the perturbative one-gluon exchange interaction. Herein, the low-lying S -wave positive parity $c\bar{c}s\bar{q}$ tetraquark states shall be investigated, and thus the central and spin-spin terms of the potential are the only ones needed.

One consequence of the dynamical breaking of chiral symmetry is that Goldstone boson exchange interactions appear between constituent light quarks u, d and s . Therefore, the chiral interaction can be written as [59]:

$$V_\chi(\vec{r}_{ij}) = V_\pi(\vec{r}_{ij}) + V_\sigma(\vec{r}_{ij}) + V_K(\vec{r}_{ij}) + V_\eta(\vec{r}_{ij}), \quad (4)$$

given by

$$V_\pi(\vec{r}_{ij}) = \frac{g_{ch}^2}{4\pi} \frac{m_\pi^2}{12m_i m_j} \frac{\Lambda_\pi^2}{\Lambda_\pi^2 - m_\pi^2} m_\pi \left[Y(m_\pi r_{ij}) - \frac{\Lambda_\pi^3}{m_\pi^3} Y(\Lambda_\pi r_{ij}) \right] (\vec{\sigma}_i \cdot \vec{\sigma}_j) \sum_{a=1}^3 (\lambda_i^a \cdot \lambda_j^a), \quad (5)$$

$$V_\sigma(\vec{r}_{ij}) = -\frac{g_{ch}^2}{4\pi} \frac{\Lambda_\sigma^2}{\Lambda_\sigma^2 - m_\sigma^2} m_\sigma \left[Y(m_\sigma r_{ij}) - \frac{\Lambda_\sigma}{m_\sigma} Y(\Lambda_\sigma r_{ij}) \right], \quad (6)$$

$$\begin{aligned}
V_K(\vec{r}_{ij}) &= \frac{g_{ch}^2}{4\pi} \frac{m_K^2}{12m_i m_j} \frac{\Lambda_K^2}{\Lambda_K^2 - m_K^2} m_K \left[Y(m_K r_{ij}) \right. \\
&\quad \left. - \frac{\Lambda_K^3}{m_K^3} Y(\Lambda_K r_{ij}) \right] (\vec{\sigma}_i \cdot \vec{\sigma}_j) \sum_{a=4}^7 (\lambda_i^a \cdot \lambda_j^a), \quad (7) \\
V_\eta(\vec{r}_{ij}) &= \frac{g_{ch}^2}{4\pi} \frac{m_\eta^2}{12m_i m_j} \frac{\Lambda_\eta^2}{\Lambda_\eta^2 - m_\eta^2} m_\eta \left[Y(m_\eta r_{ij}) \right. \\
&\quad \left. - \frac{\Lambda_\eta^3}{m_\eta^3} Y(\Lambda_\eta r_{ij}) \right] (\vec{\sigma}_i \cdot \vec{\sigma}_j) \left[\cos \theta_p (\lambda_i^8 \cdot \lambda_j^8) \right. \\
&\quad \left. - \sin \theta_p \right], \quad (8)
\end{aligned}$$

where $Y(x) = e^{-x}/x$ is the standard Yukawa function. The physical η meson, instead of the octet one, is considered by introducing the angle θ_p . The λ^a are the SU(3) flavor Gell-Mann matrices. Taken from their experimental values, m_π , m_K and m_η are the masses of the SU(3) Goldstone bosons. The value of m_σ is determined through the PCAC relation $m_\sigma^2 \simeq m_\pi^2 + 4m_{u,d}^2$ [60]. Finally, the chiral coupling constant, g_{ch} , is determined from the πNN coupling constant through

$$\frac{g_{ch}^2}{4\pi} = \frac{9}{25} \frac{g_{\pi NN}^2}{4\pi} \frac{m_{u,d}^2}{m_N^2}, \quad (9)$$

which assumes that flavor SU(3) is an exact symmetry only broken by the different mass of the strange quark. Herein, we should notice that only one \bar{q} ($q = u, d$) and one s light quark is considered in the tetraquark system, hence the π -meson exchange potential will be excluded in the chiral interaction.

Color confinement should be encoded in the non-Abelian character of QCD. It has been demonstrated by lattice-regularized QCD that multi-gluon exchanges produce an attractive linearly rising potential proportional to the distance between infinite-heavy quarks [61]. However, the spontaneous creation of light-quark pairs from the QCD vacuum may give rise at the same scale to a breakup of the created color flux-tube [61]. These two observations can be described phenomenologically by

$$V_{\text{CON}}(\vec{r}_{ij}) = [-a_c(1 - e^{-\mu_c r_{ij}}) + \Delta] (\lambda_i^c \cdot \lambda_j^c), \quad (10)$$

where a_c , μ_c and Δ are model parameters,¹ and the SU(3) color Gell-Mann matrices are denoted as λ^c . One can see in Eq. (10) that the potential is linear at short inter-quark distances with an effective confinement strength $\sigma = -a_c \mu_c (\lambda_i^c \cdot \lambda_j^c)$, while it becomes constant at large distances, $V_{\text{thr.}} = (\Delta - a_c)(\lambda_i^c \cdot \lambda_j^c)$.

Beyond the chiral symmetry breaking scale one expects the dynamics to be governed by QCD perturbative

TABLE I. Model parameters.

Quark masses	m_q ($q = u, d$) (MeV)	313
	m_s (MeV)	555
	m_c (MeV)	1752
Goldstone bosons	Λ_σ (fm ⁻¹)	4.20
	$\Lambda_\eta = \Lambda_K$ (fm ⁻¹)	5.20
	$g_{ch}^2/(4\pi)$	0.54
	θ_P (°)	-15
Confinement	a_c (MeV)	430
	μ_c (fm ⁻¹)	0.70
	Δ (MeV)	181.10
OGE	α_0	2.118
	Λ_0 (fm ⁻¹)	0.113
	μ_0 (MeV)	36.976
	\hat{r}_0 (MeV fm)	28.170

effects. In particular, the one-gluon exchange potential (which includes the so-called coulomb and color-magnetic interactions) is the leading order contribution:

$$\begin{aligned}
V_{\text{OGE}}(\vec{r}_{ij}) &= \frac{1}{4} \alpha_s (\lambda_i^c \cdot \lambda_j^c) \left[\frac{1}{r_{ij}} \right. \\
&\quad \left. - \frac{1}{6m_i m_j} (\vec{\sigma}_i \cdot \vec{\sigma}_j) \frac{e^{-r_{ij}/r_0(\mu_{ij})}}{r_{ij} r_0^2(\mu_{ij})} \right], \quad (11)
\end{aligned}$$

where $r_0(\mu_{ij}) = \hat{r}_0/\mu_{ij}$ is a regulator which depends on the reduced mass of the $q\bar{q}$ pair, the Pauli matrices are denoted by $\vec{\sigma}$, and the contact term has been regularized as

$$\delta(\vec{r}_{ij}) \sim \frac{1}{4\pi r_0^2(\mu_{ij})} \frac{e^{-r_{ij}/r_0(\mu_{ij})}}{r_{ij}}. \quad (12)$$

An effective scale-dependent strong coupling constant, $\alpha_s(\mu_{ij})$, provides a consistent description of mesons and baryons from light to heavy quark sectors. We use the definition of Ref. [44]:

$$\alpha_s(\mu_{ij}) = \frac{\alpha_0}{\ln\left(\frac{\mu_{ij}^2 + \mu_0^2}{\Lambda_0^2}\right)}, \quad (13)$$

in which α_0 , μ_0 and Λ_0 are parameters of the model.

The model parameters are listed in Table I. Additionally, for later concern, Table II lists theoretical and experimental (if available) masses of $1S$ and $2S$ states of $K^{(*)}$, $D^{(*)}$, $D_s^{(*)}$, η_c and J/ψ mesons predicted within our theoretical framework.

Figure 1 shows seven kinds of configurations for the $c\bar{c}s\bar{q}$ tetraquark system. In particular, Fig. 1(a) and Fig. 1(b) are meson-meson structures, Fig. 1(c) is the diquark-antidiquark one, and the other K-type configurations are from panels (d) to (g). All of them, and their

¹ It is widely believed that confinement is flavor independent and thus it should be constraint by the light hadron spectra despite our aim is to determine energy states in heavier quark sectors [43, 62]

TABLE II. Theoretical and experimental (if available) masses of $nL = 1S$ and $2S$ states of $K^{(*)}$, $D^{(*)}$, $D_s^{(*)}$, η_c and J/ψ mesons.

Meson	nL	$M_{\text{The.}}$ (MeV)	$M_{\text{Exp.}}$ (MeV)
K	$1S$	481	494
	$2S$	1468	-
K^*	$1S$	907	892
	$2S$	1621	-
D	$1S$	1897	1870
	$2S$	2648	-
D^*	$1S$	2017	2007
	$2S$	2704	-
D_s	$1S$	1989	1968
	$2S$	2705	-
D_s^*	$1S$	2115	2112
	$2S$	2769	-
η_c	$1S$	2989	2981
	$2S$	3627	-
J/ψ	$1S$	3097	3097
ψ	$2S$	3685	-

couplings, are considered in our investigation. However, for the purpose of solving a manageable 4-body problem, the K-type configurations are sometimes restricted. It is important to note herein that just one configuration would be enough for the calculation, if all radial and orbital excited states were taken into account; however, this is obviously much less efficient and thus an economic way is to combine the different configurations in the ground state to perform the calculation.

The multiquark system's wave function at the quark level is an internal product of color, spin, flavor and space terms. Concerning the color degree-of-freedom, the colorless wave function of a 4-quark system in meson-meson configuration, as illustrated in Fig. 1(a) and Fig. 1(b), can be obtained by either two coupled color-singlet clusters, $1 \otimes 1$:

$$\chi_1^c = \frac{1}{3}(\bar{r}r + \bar{g}g + \bar{b}b) \times (\bar{r}r + \bar{g}g + \bar{b}b), \quad (14)$$

or two coupled color-octet clusters, $8 \otimes 8$:

$$\begin{aligned} \chi_2^c = & \frac{\sqrt{2}}{12}(3\bar{b}r\bar{r}b + 3\bar{g}r\bar{r}g + 3\bar{b}g\bar{g}b + 3\bar{g}b\bar{b}g + 3\bar{r}g\bar{g}r \\ & + 3\bar{r}b\bar{b}r + 2\bar{r}r\bar{r}r + 2\bar{g}g\bar{g}g + 2\bar{b}b\bar{b}b - \bar{r}r\bar{g}g \\ & - \bar{g}g\bar{r}r - \bar{b}b\bar{g}g - \bar{b}b\bar{r}r - \bar{g}g\bar{b}b - \bar{r}r\bar{b}b). \end{aligned} \quad (15)$$

These two color states are the so-called color-singlet and hidden-color channels, respectively.

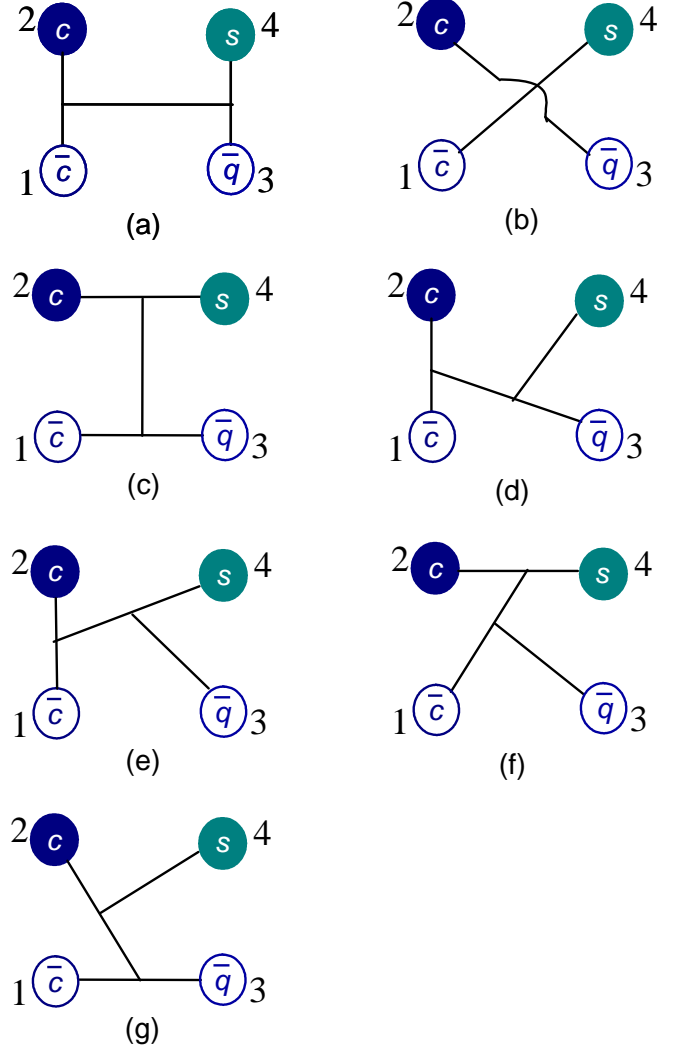


FIG. 1. Seven types of configurations in $c\bar{c}s\bar{q}$ ($q = u, d$) tetraquarks. Panel (a) and (b) are meson-meson structures, panel (c) is diquark-antidiquark one and the other K-type structures are from panel (d) to (g).

The color wave functions associated to the diquark-antidiquark structure shown in Fig. 1(c) are the coupled color triplet-antitriplet clusters, $3 \otimes \bar{3}$:

$$\begin{aligned} \chi_3^c = & \frac{\sqrt{3}}{6}(\bar{r}r\bar{g}g - \bar{g}r\bar{r}g + \bar{g}g\bar{r}r - \bar{r}g\bar{g}r + \bar{r}r\bar{b}b \\ & - \bar{b}r\bar{r}b + \bar{b}b\bar{r}r - \bar{r}b\bar{b}r + \bar{g}g\bar{b}b - \bar{b}g\bar{g}b \\ & + \bar{b}b\bar{g}g - \bar{g}b\bar{b}g), \end{aligned} \quad (16)$$

and the coupled color sextet-antisextet clusters, $6 \otimes \bar{6}$:

$$\begin{aligned} \chi_4^c = & \frac{\sqrt{6}}{12}(2\bar{r}r\bar{r}r + 2\bar{g}g\bar{g}g + 2\bar{b}b\bar{b}b + \bar{r}r\bar{g}g + \bar{g}r\bar{r}g \\ & + \bar{g}g\bar{r}r + \bar{r}g\bar{g}r + \bar{r}r\bar{b}b + \bar{b}r\bar{r}b + \bar{b}b\bar{r}r \\ & + \bar{r}b\bar{b}r + \bar{g}g\bar{b}b + \bar{b}g\bar{g}b + \bar{b}b\bar{g}g + \bar{g}b\bar{b}g). \end{aligned} \quad (17)$$

Meanwhile, the colorless wave functions of the K-type

structures shown in Fig. 1(d) to (g) are

$$\begin{aligned} \chi_5^c = & \frac{1}{6\sqrt{2}}(\bar{r}r\bar{r}r + \bar{g}g\bar{g}g - 2\bar{b}b\bar{b}b) + \\ & \frac{1}{2\sqrt{2}}(\bar{r}b\bar{b}r + \bar{r}g\bar{g}r + \bar{g}b\bar{b}g + \bar{g}r\bar{r}g + \bar{b}g\bar{g}b + \bar{b}r\bar{r}b) - \\ & \frac{1}{3\sqrt{2}}(\bar{g}g\bar{r}r + \bar{r}r\bar{g}g) + \frac{1}{6\sqrt{2}}(\bar{b}b\bar{r}r + \bar{b}b\bar{g}g + \bar{r}r\bar{b}b + \bar{g}g\bar{b}b), \end{aligned} \quad (18)$$

$$\chi_6^c = \chi_1^c, \quad (19)$$

$$\chi_7^c = \chi_1^c, \quad (20)$$

$$\begin{aligned} \chi_8^c = & \frac{1}{4}\left(1 - \frac{1}{\sqrt{6}}\right)\bar{r}r\bar{g}g - \frac{1}{4}\left(1 + \frac{1}{\sqrt{6}}\right)\bar{g}g\bar{g}g - \frac{1}{4\sqrt{3}}\bar{r}g\bar{g}r + \\ & \frac{1}{2\sqrt{2}}(\bar{r}b\bar{b}r + \bar{g}b\bar{b}g + \bar{b}g\bar{g}b + \bar{g}r\bar{r}g + \bar{b}r\bar{r}b) + \\ & \frac{1}{2\sqrt{6}}(\bar{r}r\bar{b}b - \bar{g}g\bar{b}b + \bar{b}b\bar{g}g + \bar{g}g\bar{r}r - \bar{b}b\bar{r}r), \end{aligned} \quad (21)$$

$$\begin{aligned} \chi_9^c = & \frac{1}{2\sqrt{6}}(\bar{r}b\bar{b}r + \bar{r}r\bar{b}b + \bar{g}b\bar{b}g + \bar{g}g\bar{b}b + \bar{r}g\bar{g}r + \bar{r}r\bar{g}g + \\ & \bar{b}b\bar{g}g + \bar{b}g\bar{g}b + \bar{g}g\bar{r}r + \bar{g}r\bar{r}g + \bar{b}b\bar{r}r + \bar{b}r\bar{r}b) + \\ & \frac{1}{\sqrt{6}}(\bar{r}r\bar{r}r + \bar{g}g\bar{g}g + \bar{b}b\bar{b}b), \end{aligned} \quad (22)$$

$$\begin{aligned} \chi_{10}^c = & \frac{1}{2\sqrt{3}}(\bar{r}b\bar{b}r - \bar{r}r\bar{b}b + \bar{g}b\bar{b}g - \bar{g}g\bar{b}b + \bar{r}g\bar{g}r - \bar{r}r\bar{g}g - \\ & \bar{b}b\bar{g}g + \bar{b}g\bar{g}b - \bar{g}g\bar{r}r + \bar{g}r\bar{r}g - \bar{b}b\bar{r}r + \bar{b}r\bar{r}b), \end{aligned} \quad (23)$$

$$\chi_{11}^c = \chi_9^c, \quad (24)$$

$$\chi_{12}^c = -\chi_{10}^c. \quad (25)$$

As for the flavor degree-of-freedom, since the quark content of the investigated tetraquark system is $c\bar{c}s\bar{q}$ ($q = u, d$), only $I = 1/2$ sector is discussed. The flavor wavefunction is denoted as χ_{I, M_I}^f , where the third component of the isospin, M_I , is fixed to be equal to I for simplicity, since the Hamiltonian does not have a flavor-dependent interaction which can distinguish the third component of the isospin quantum number.

We are going to consider S -wave ground states with spin ranging from $S = 0$ to 2. Therefore, the spin wave functions, χ_{S, M_S}^σ , are given by (M_S can be set to be equal

to S without loss of generality):

$$\chi_{0,0}^{\sigma u_1}(4) = \chi_{00}^\sigma \chi_{00}^\sigma, \quad (26)$$

$$\chi_{0,0}^{\sigma u_2}(4) = \frac{1}{\sqrt{3}}(\chi_{11}^\sigma \chi_{1,-1}^\sigma - \chi_{10}^\sigma \chi_{10}^\sigma + \chi_{1,-1}^\sigma \chi_{11}^\sigma), \quad (27)$$

$$\begin{aligned} \chi_{0,0}^{\sigma u_3}(4) = & \frac{1}{\sqrt{2}}\left(\left(\sqrt{\frac{2}{3}}\chi_{11}^\sigma \chi_{\frac{1}{2},-\frac{1}{2}}^\sigma - \sqrt{\frac{1}{3}}\chi_{10}^\sigma \chi_{\frac{1}{2},\frac{1}{2}}^\sigma\right)\chi_{\frac{1}{2},-\frac{1}{2}}^\sigma \right. \\ & \left. - \left(\sqrt{\frac{1}{3}}\chi_{10}^\sigma \chi_{\frac{1}{2},-\frac{1}{2}}^\sigma - \sqrt{\frac{2}{3}}\chi_{1,-1}^\sigma \chi_{\frac{1}{2},\frac{1}{2}}^\sigma\right)\chi_{\frac{1}{2},\frac{1}{2}}^\sigma\right), \end{aligned} \quad (28)$$

$$\chi_{0,0}^{\sigma u_4}(4) = \frac{1}{\sqrt{2}}(\chi_{00}^\sigma \chi_{\frac{1}{2},\frac{1}{2}}^\sigma \chi_{\frac{1}{2},-\frac{1}{2}}^\sigma - \chi_{00}^\sigma \chi_{\frac{1}{2},-\frac{1}{2}}^\sigma \chi_{\frac{1}{2},\frac{1}{2}}^\sigma), \quad (29)$$

$$\chi_{1,1}^{\sigma w_1}(4) = \chi_{00}^\sigma \chi_{11}^\sigma, \quad (30)$$

$$\chi_{1,1}^{\sigma w_2}(4) = \chi_{11}^\sigma \chi_{00}^\sigma, \quad (31)$$

$$\chi_{1,1}^{\sigma w_3}(4) = \frac{1}{\sqrt{2}}(\chi_{11}^\sigma \chi_{10}^\sigma - \chi_{10}^\sigma \chi_{11}^\sigma), \quad (32)$$

$$\begin{aligned} \chi_{1,1}^{\sigma w_4}(4) = & \sqrt{\frac{3}{4}}\chi_{11}^\sigma \chi_{\frac{1}{2},\frac{1}{2}}^\sigma \chi_{\frac{1}{2},-\frac{1}{2}}^\sigma - \sqrt{\frac{1}{12}}\chi_{11}^\sigma \chi_{\frac{1}{2},-\frac{1}{2}}^\sigma \chi_{\frac{1}{2},\frac{1}{2}}^\sigma \\ & - \sqrt{\frac{1}{6}}\chi_{10}^\sigma \chi_{\frac{1}{2},\frac{1}{2}}^\sigma \chi_{\frac{1}{2},\frac{1}{2}}^\sigma, \end{aligned} \quad (33)$$

$$\chi_{1,1}^{\sigma w_5}(4) = \left(\sqrt{\frac{2}{3}}\chi_{11}^\sigma \chi_{\frac{1}{2},-\frac{1}{2}}^\sigma - \sqrt{\frac{1}{3}}\chi_{10}^\sigma \chi_{\frac{1}{2},\frac{1}{2}}^\sigma\right)\chi_{\frac{1}{2},\frac{1}{2}}^\sigma, \quad (34)$$

$$\chi_{1,1}^{\sigma w_6}(4) = \chi_{00}^\sigma \chi_{\frac{1}{2},\frac{1}{2}}^\sigma \chi_{\frac{1}{2},\frac{1}{2}}^\sigma, \quad (35)$$

$$\chi_{2,2}^{\sigma 1}(4) = \chi_{11}^\sigma \chi_{11}^\sigma. \quad (36)$$

The superscripts u_1, \dots, u_4 and w_1, \dots, w_6 determine the spin wave function for each configuration of the $c\bar{c}s\bar{q}$ tetraquark system, their specific values are shown in Table III. Furthermore, the expressions above are obtained by considering the coupling of two sub-clusters whose spin wave functions are given by trivial SU(2) algebra, and the necessary basis reads as

$$\chi_{11}^\sigma = \chi_{\frac{1}{2},\frac{1}{2}}^\sigma \chi_{\frac{1}{2},\frac{1}{2}}^\sigma, \quad (37)$$

$$\chi_{1,-1}^\sigma = \chi_{\frac{1}{2},-\frac{1}{2}}^\sigma \chi_{\frac{1}{2},-\frac{1}{2}}^\sigma, \quad (38)$$

$$\chi_{10}^\sigma = \frac{1}{\sqrt{2}}(\chi_{\frac{1}{2},\frac{1}{2}}^\sigma \chi_{\frac{1}{2},-\frac{1}{2}}^\sigma + \chi_{\frac{1}{2},-\frac{1}{2}}^\sigma \chi_{\frac{1}{2},\frac{1}{2}}^\sigma), \quad (39)$$

$$\chi_{00}^\sigma = \frac{1}{\sqrt{2}}(\chi_{\frac{1}{2},\frac{1}{2}}^\sigma \chi_{\frac{1}{2},-\frac{1}{2}}^\sigma - \chi_{\frac{1}{2},-\frac{1}{2}}^\sigma \chi_{\frac{1}{2},\frac{1}{2}}^\sigma), \quad (40)$$

Among the different methods to solve the Schrödinger-like 4-body bound state equation, we use the Rayleigh-Ritz variational principle which is one of the most extended tools to solve eigenvalue problems because its simplicity and flexibility. Moreover, we use the complex-range method and thus the spatial wave function is written as follows:

$$\psi_{LM_L}(\theta) = \left[\left[\phi_{n_1 l_1}(\vec{\rho} e^{i\theta}) \phi_{n_2 l_2}(\vec{\lambda} e^{i\theta}) \right]_l \phi_{n_3 l_3}(\vec{R} e^{i\theta}) \right]_{LM_L}, \quad (41)$$

TABLE III. The values of the superscripts u_1, \dots, u_4 and w_1, \dots, w_6 that determine the spin wave function for each configuration of the $c\bar{c}s\bar{q}$ tetraquark system.

	Di-meson	Diquark-antidiquark	K_1	K_2	K_3	K_4
u_1	1	3				
u_2	2	4				
u_3			5	7	9	11
u_4			6	8	10	12
w_1	1	4				
w_2	2	5				
w_3	3	6				
w_4			7	10	13	16
w_5			8	11	14	17
w_6			9	12	15	18

where the internal Jacobi coordinates are defined as

$$\vec{\rho} = \vec{x}_1 - \vec{x}_{2(4)}, \quad (42)$$

$$\vec{\lambda} = \vec{x}_3 - \vec{x}_{4(2)}, \quad (43)$$

$$\vec{R} = \frac{m_1\vec{x}_1 + m_{2(4)}\vec{x}_{2(4)}}{m_1 + m_{2(4)}} - \frac{m_3\vec{x}_3 + m_{4(2)}\vec{x}_{4(2)}}{m_3 + m_{4(2)}}, \quad (44)$$

for the meson-meson configurations of Fig. 1(a) and 1(b), where the numbers in parentheses are those corresponding to Fig. 1(b); and as

$$\vec{\rho} = \vec{x}_1 - \vec{x}_3, \quad (45)$$

$$\vec{\lambda} = \vec{x}_2 - \vec{x}_4, \quad (46)$$

$$\vec{R} = \frac{m_1\vec{x}_1 + m_3\vec{x}_3}{m_1 + m_3} - \frac{m_2\vec{x}_2 + m_4\vec{x}_4}{m_2 + m_4}, \quad (47)$$

for the diquark-antidiquark structure of Fig. 1(c). The remaining K-type configurations shown in Fig. 1(d) to 1(g) are (i, j, k, l) take values according to the panels (d) to (g) of Fig. 1):

$$\vec{\rho} = \vec{x}_i - \vec{x}_j, \quad (48)$$

$$\vec{\lambda} = \vec{x}_k - \frac{m_i\vec{x}_i + m_j\vec{x}_j}{m_i + m_j}, \quad (49)$$

$$\vec{R} = \vec{x}_l - \frac{m_i\vec{x}_i + m_j\vec{x}_j + m_k\vec{x}_k}{m_i + m_j + m_k}. \quad (50)$$

It becomes obvious now that the center-of-mass kinetic term, T_{CM} , can be completely eliminated for a non-relativistic system defined in any of the above sets of relative coordinates.

A crucial aspect of the Rayleigh-Ritz variational method is the basis expansion of the trial wave function. We are going to use the Gaussian expansion method (GEM) [56] in which each relative coordinate is expanded in terms of Gaussian basis functions whose sizes are taken in geometric progression. This method has proven to be

very efficient on solving the bound-state problem of multi-quark systems [33–38, 55] and the details on how the geometric progression is fixed can be found in, *e.g.* Ref. [33]. Therefore, the form of the orbital wave functions, ϕ 's, in Eq. (41) is

$$\phi_{nlm}(\vec{r}e^{i\theta}) = N_{nl}(re^{i\theta})^l e^{-\nu_n(re^{i\theta})^2} Y_{lm}(\hat{r}). \quad (51)$$

Since only S -wave states of charm(bottom)-strange tetraquarks are investigated in this work, no laborious Racah algebra is needed while computing matrix elements. In this case, the value of the spherical harmonic function is just a constant, *viz.* $Y_{00} = \sqrt{1/4\pi}$.

Finally, the complete wave-function that fulfills the Pauli principle is written as

$$\Psi_{JMJ,I,i,j,k}(\theta) = \mathcal{A} \left[[\psi_L(\theta)\chi_S^{\sigma_i}(4)]_{JM_J} \chi_I^{f_j} \chi_k^c \right], \quad (52)$$

where \mathcal{A} is the antisymmetry operator of $c\bar{c}s\bar{q}$ tetraquark system and it just reads $\mathcal{A} = 1$, since each of the four particles are nonidentical.

III. RESULTS

In the present calculation, we investigate all possible S -wave hidden-charm tetraquarks with strangeness by taking into account di-meson, diquark-antidiquark and K-type configurations. In our approach, a $c\bar{c}s\bar{q}$ tetraquark state has positive parity assuming that the angular momenta l_1 , l_2 and l_3 in Eq. (41) are all equal to zero. Accordingly, the total angular momentum, J , coincides with the total spin, S , and can take values 0, 1 and 2. Besides, the value of isospin, I , can only be 1/2 considering the quark content of the $c\bar{c}s\bar{q}$ system.

Tables IV, V and VI list the allowed meson-meson, diquark-antidiquark and K-type channels; they are indexed in the first column, particular combinations of spin ($\chi_J^{\sigma_i}$), flavor ($\chi_I^{f_j}$) and color (χ_k^c) wave functions are shown in the second column, and the last column reflects the specific physical channel.

Let us proceed now to describe in detail our theoretical findings for each $J^P = 0^+, 1^+$ and 2^+ sector of $c\bar{c}s\bar{q}$ tetraquarks. Three subsections are presented in the following and, in order to explore the detailed nature of the found states, three kinds of calculations are performed, *i.e.* the $(c\bar{c})(s\bar{q})$ di-meson configuration along with diquark-antidiquark and K-type ones in a coupled-channels study, the $(c\bar{q})(s\bar{c})$ di-meson configuration coupled with the other two types of exotic structures, and a complete coupled-channels investigation.

A. The $J^P = 0^+$ $c\bar{c}s\bar{q}$ tetraquark system

Table VII shows our calculated results of the lowest-lying $c\bar{c}s\bar{q}$ tetraquark states in real-range study. The allowed dimeson, diquark-antidiquark and K-type configurations are listed in the 1st column; when possible, the

TABLE IV. All possible channels for $J^P = 0^+ c\bar{c}s\bar{q}$ tetraquark system. The second column shows the necessary basis combination in spin ($\chi_J^{\sigma_i}$), flavor ($\chi_I^{f_j}$) and color (χ_k^c) degrees of freedom. Particularly, the flavor index (j) 1 is of $c\bar{c}q\bar{s}$ and 2 is of $\bar{c}s\bar{q}c$, respectively. The superscript 1 and 8 stands for the color-singlet and hidden-color configurations of physical channels.

Index	$\chi_J^{\sigma_i}; \chi_I^{f_j}; \chi_k^c$ [$i; j; k$]	Channel
1	[1; 1; 1]	$(\eta_c K)^1$
2	[2; 1; 1]	$(J/\psi K^*)^1$
3	[1; 2; 1]	$(DD_s)^1$
4	[2; 2; 1]	$(D^* D_s^*)^1$
5	[1; 1; 2]	$(\eta_c K)^8$
6	[2; 1; 2]	$(J/\psi K^*)^8$
7	[1; 2; 2]	$(DD_s)^8$
8	[2; 2; 2]	$(D^* D_s^*)^8$
9	[3; 1; 3]	$(cs)_3(\bar{c}\bar{q})_{\bar{3}}$
10	[4; 1; 3]	$(cs)_3^*(\bar{c}\bar{q})_{\bar{3}}^*$
11	[3; 1; 4]	$(cs)_6(\bar{c}\bar{q})_{\bar{6}}$
12	[4; 1; 4]	$(cs)_6^*(\bar{c}\bar{q})_{\bar{6}}^*$
13	[5; 1; 5]	K_1
14	[6; 1; 5]	K_1
15	[5; 1; 6]	K_1
16	[6; 1; 6]	K_1
17	[7; 1; 7]	K_2
18	[8; 1; 7]	K_2
19	[7; 1; 8]	K_2
20	[8; 1; 8]	K_2
21	[9; 1; 9]	K_3
22	[10; 1; 9]	K_3
23	[9; 1; 10]	K_3
24	[10; 1; 10]	K_3
25	[11; 1; 11]	K_4
26	[12; 1; 11]	K_4
27	[11; 1; 12]	K_4
28	[12; 1; 12]	K_4

experimental value of the non-interacting meson-meson threshold is labeled in parentheses. Each channel is assigned an index in the 2nd column. The theoretical mass obtained in each channel is shown in the 3rd column and the coupled-channels result for each kind of configuration is presented in the last one. When a complete coupled-channels calculation is performed, last row of the table indicates the lowest-lying mass. We show in Figs. 2 to 4 the distribution of complex eigen-energies when the CSM is used in the coupled-channels calculation and, therein, the obtained resonance states are indicated inside circles. Furthermore, when all channels listed in Table IV are considered excluding the di-meson states in color-singlet configurations, the obtained resonances below 4.3 GeV

along with their inner structures are summarized in Table VIII.

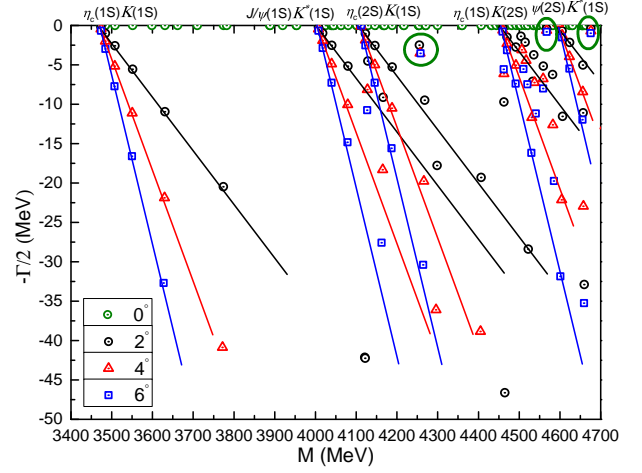


FIG. 2. The coupled-channels calculation of the $c\bar{c}s\bar{q}$ tetraquark system with $J^P = 0^+$ quantum numbers. Particularly, the $(c\bar{c})(s\bar{q})$ dimeson channels are excluded. We use the complex-scaling method of the chiral quark model varying θ from 0° to 6° .

Exotic states in $(c\bar{c})(s\bar{q})$ dimeson channels: In Table VII shows that the lowest channel of $c\bar{c}s\bar{q}$ tetraquark with spin-parity 0^+ is the color-singlet channel of $\eta_c K$ with a theoretical mass of 3470 MeV, which is just the theoretical threshold value and thus bounding is impossible here. This fact also holds for another higher meson-meson channel, $J/\psi K^*$, whose calculated mass is 4004 MeV. Then, the hidden-color structures for $\eta_c K$ and $J/\psi K^*$ have masses 4422 and 4416 MeV, respectively; obviously, these are much deviated from the relevant experimental data.

A coupled-channels within complex-range calculation is performed in a further step. Fig. 2 presents the calculated results, in which the $(c\bar{c})(s\bar{q})$ dimeson, diquark-antidiquark and K-type configurations are considered. In a mass gap from 3.4 to 4.7 GeV, the calculated complex energy dots of $\eta_c(1S)K(1S)$, $J/\psi(1S)K^*(1S)$, $\eta_c(2S)K(1S)$, $\eta_c(1S)K(2S)$ and $\psi(2S)K^*(1S)$ channels are generally well aligned along their corresponding threshold lines. In particular, with a complex angle varied from 0° to 6° , these energy poles are basically moving along the theoretical cut lines, and this fact confirms their nature as scattering states. In Fig. 2 one could find that three resonance poles exist, circled in green, whose masses and widths are (4255, 5.0) MeV, (4567, 1.6) MeV and (4675, 1.9) MeV, respectively. These narrow resonances are obtained in the $(c\bar{c})(s\bar{q})$ dimeson channels along with the couplings in diquark-antidiquark and K-type configurations. Moreover, attending to their positions in the complex plane, the dominant components of them can be identified as $\eta_c(2S)K(1S)$ (4255), $\eta_c(1S)K(2S)$ (4567) and $\psi(2S)K^*(1S)$ (4675), respectively. Accordingly, the re-

TABLE V. All possible channels for $J^P = 1^+ c\bar{c}s\bar{q}$ tetraquark system. The second and fifth columns show the necessary basis combination in spin ($\chi_J^{\sigma_i}$), flavor ($\chi_I^{f_j}$) and color (χ_k^c) degrees of freedom. Particularly, the flavor indices (j) 1 is of $\bar{c}c\bar{q}s$ and 2 is of $\bar{c}s\bar{q}c$, respectively. The superscript 1 and 8 stands for the color-singlet and hidden-color configurations of physical channels.

Index	$\chi_J^{\sigma_i}; \chi_I^{f_j}; \chi_k^c$ [$i; j; k$]	Channel	Index	$\chi_J^{\sigma_i}; \chi_I^{f_j}; \chi_k^c$ [$i; j; k$]	Channel
1	[1; 1; 1]	$(\eta_c K^*)^1$	19	[7; 1; 5]	K_1
2	[2; 1; 1]	$(J/\psi K)^1$	20	[8; 1; 5]	K_1
3	[3; 1; 1]	$(J/\psi K^*)^1$	21	[9; 1; 5]	K_1
4	[1; 2; 1]	$(DD_s^*)^1$	22	[7; 1; 6]	K_1
5	[2; 2; 1]	$(D^* D_s)^1$	23	[8; 1; 6]	K_1
6	[3; 2; 1]	$(D^* D_s^*)^1$	24	[9; 1; 6]	K_1
7	[1; 1; 2]	$(\eta_c K^*)^8$	25	[10; 1; 7]	K_2
8	[2; 1; 2]	$(J/\psi K)^8$	26	[11; 1; 7]	K_2
9	[3; 1; 2]	$(J/\psi K^*)^8$	27	[12; 1; 7]	K_2
10	[1; 2; 2]	$(DD_s^*)^8$	28	[10; 1; 8]	K_2
11	[2; 2; 2]	$(D^* D_s)^8$	29	[11; 1; 8]	K_2
12	[3; 2; 2]	$(D^* D_s^*)^8$	30	[12; 1; 8]	K_2
13	[4; 1; 3]	$(cs)_3(\bar{c}\bar{q})_3^*$	31	[13; 1; 9]	K_3
14	[5; 1; 3]	$(cs)_3^*(\bar{c}\bar{q})_3$	32	[14; 1; 9]	K_3
15	[6; 1; 3]	$(cs)_3^*(\bar{c}\bar{q})_3^*$	33	[15; 1; 9]	K_3
16	[4; 1; 4]	$(cs)_6(\bar{c}\bar{q})_6^*$	34	[13; 1; 10]	K_3
17	[5; 1; 4]	$(cs)_6^*(\bar{c}\bar{q})_6$	35	[14; 1; 10]	K_3
18	[6; 1; 4]	$(cs)_6^*(\bar{c}\bar{q})_6^*$	36	[15; 1; 10]	K_3
			37	[16; 1; 11]	K_4
			38	[17; 1; 11]	K_4
			39	[18; 1; 11]	K_4
			40	[16; 1; 12]	K_4
			41	[17; 1; 12]	K_4
			42	[18; 1; 12]	K_4

ported $Z_{cs}(4220)$ and $X(4630)$ states can be related to the radial excitation of $\eta_c K$ and ψK^* in coupled-channels cases, without $D^{(*)}D_s^{(*)}$ channel included.

Exotic states in $(c\bar{q})(s\bar{c})$ dimeson channels: In a single channel calculation of $(c\bar{q})(s\bar{c})$ meson-meson configuration, the lowest mass 3886 MeV is equal to the theoretical threshold value of DD_s color-singlet channel in Table VII, and the other $(c\bar{q})(s\bar{c})$ dimeson channel, $D^*D_s^*$, is at 4132 MeV. Therefore, no bound state is found herein too, since the color-octet channels of DD_s and $D^*D_s^*$ are both excited states at around 4.3 GeV.

In a further step, a coupled-channels calculation which includes the $(c\bar{q})(s\bar{c})$ dimeson, diquark-antidiquark and K-type configurations is considered in the CSM. Fig. 3 presents the general distributions of calculated complex energy dots. Particularly, in the top panel of Fig. 3, most of the complex poles of $D^{(*)}D_s^{(*)}$ are aligned well along the cut lines within a mass region from 3.8 to 4.7 GeV. However, there are dense distributions around 4.2 and 4.6 GeV, and so two enlarged panels are shown accordingly. Firstly, two resonance poles are obtained in the

middle panel of Fig. 3 whose mass gap ranges from 4.10 to 4.25 GeV. They can be identified as $D^*(1S)D_s^*(1S)$ narrow resonances with calculated masses and widths (4150, 2.2) MeV and (4185, 8.2) MeV, respectively. For the lower resonance, despite its small decay width, our theoretical mass is compatible with the $Z'_{cs}(4130)$ (tensor $D^*\bar{D}_s^*$ resonance) concluded by Refs. [4, 25].

The bottom panel of Fig. 3 shows the highest energy region, 4.55~4.70 GeV, where the radial excitations of DD_s thresholds are clearly identified. Therein, the calculated complex dots are generally aligned along their corresponding threshold lines, and no stable resonance pole is found.

The fully coupled-channels case: There are 28 channels under consideration for the $c\bar{c}s\bar{q}$ tetraquark with spin-parity 0^+ . In Table VII one could see that, apart from the dimeson channels in both color-singlet and -octet cases, four allowed channels in diquark-antidiquark and K-type configurations are also considered. Generally, in each single channel computation, masses of diquark-antidiquark structures are about 4.3 GeV, and 4.1~4.4 GeV for K-type ones. Then, in coupled-channels calcu-

TABLE VI. All possible channels for $J^P = 2^+ c\bar{c}s\bar{q}$ tetraquark system. The second column shows the necessary basis combination in spin ($\chi_J^{\sigma_i}$), flavor ($\chi_I^{f_j}$) and color (χ_k^c) degrees of freedom. Particularly, the flavor indices (j) 1 is of $c\bar{c}q\bar{s}$ and 2 is of $\bar{c}s\bar{q}c$, respectively. The superscript 1 and 8 stands for the color-singlet and hidden-color configurations of physical channels.

Index	$\chi_J^{\sigma_i}; \chi_I^{f_j}; \chi_k^c$ [$i; j; k$]	Channel
1	[1; 1; 1]	$(J/\psi K^*)^1$
2	[1; 2; 1]	$(D^* D_s^*)^1$
3	[1; 1; 2]	$(J/\psi K^*)^8$
4	[1; 2; 2]	$(D^* D_s^*)^8$
5	[1; 1; 3]	$(cs)_3^*(\bar{c}\bar{q})_3^*$
6	[1; 1; 4]	$(cs)_6^*(\bar{c}\bar{q})_6^*$
7	[1; 1; 5]	K_1
8	[1; 1; 6]	K_1
9	[1; 1; 7]	K_2
10	[1; 1; 8]	K_2
11	[1; 1; 9]	K_3
12	[1; 1; 10]	K_3
13	[1; 1; 11]	K_4
14	[1; 1; 12]	K_4

lations of each specific configurations, the lowest mass, 3470 MeV, is still just the theoretical threshold value of $\eta_c K$, and the other exotic structures are around 4.1 GeV. In particular, the coupled masses in K_1 and K_2 structures are both ~ 4.05 GeV, which is close to the experimental mass of $Z_{cs}(4000)$. Finally, within the real-range investigation, the fully coupled-channels mass remains at 3470 MeV which implies the coupling effect is quite weak and no bound state is available.

The exotic state within hidden-color channel could be a natural bound state, hence a coupled-channels calculation of all those exotic structures which include color-octet, diquark-antidiquark and K-type configurations are performed. Table VIII lists the obtained $c\bar{c}s\bar{q}$ tetraquark resonances below 4.3 GeV, and their inner structures are also investigated. The lowest resonance is at 3841 MeV, and the other four excited states are lying in 4.11~4.25 GeV. Apparently, these exotic resonance states are likely compact structures with inter-quark distance generally less than 1.1 fm, and the distance between $c\bar{c}$ is around 0.5 fm. They could be good candidates of exotic color structures in the strange hidden-charm tetraquark sector.

Additionally, the fully coupled-channels calculation is studied in a complex-range scaling. Fig. 4 shows the distribution of our calculated complex energies. Particularly, in the top panel, the scattering states of $\eta_c K$, $J/\psi K^*$, DD_s and $D^* D_s^*$ can be clearly identified within the mass region 3.4~4.7 GeV. Besides, since there is a

TABLE VII. Lowest-lying $c\bar{c}s\bar{q}$ tetraquark states with $J^P = 0^+$ calculated within the real range formulation of the chiral quark model. The allowed meson-meson, diquark-antidiquark and K-type configurations are listed in the first column; when possible, the experimental value of the non-interacting meson-meson threshold is labeled in parentheses. Each channel is assigned an index in the 2nd column. The theoretical mass obtained in each channel is shown in the 3rd column and the coupled result for each kind of configuration is presented in the last column. When a complete coupled-channels calculation is performed, last row of the table indicates the lowest-lying mass. (unit: MeV).

Channel	Index	M	Mixed
$(\eta_c K)^1(3475)$	1	3470	
$(J/\psi K^*)^1(3989)$	2	4004	
$(DD_s)^1(3838)$	3	3886	
$(D^* D_s^*)^1(4119)$	4	4132	3470
$(\eta_c K)^8$	5	4422	
$(J/\psi K^*)^8$	6	4416	
$(DD_s)^8$	7	4398	
$(D^* D_s^*)^8$	8	4333	4177
$(cs)_3(\bar{c}\bar{q})_3$	9	4320	
$(cs)_3^*(\bar{c}\bar{q})_3^*$	10	4334	
$(cs)_6(\bar{c}\bar{q})_6$	11	4349	
$(cs)_6^*(\bar{c}\bar{q})_6^*$	12	4224	4122
K_1	13	4407	
	14	4420	
	15	4296	
	16	4080	4075
K_2	17	4283	
	18	4062	
	19	4407	
	20	4419	4057
K_3	21	4217	
	22	4353	
	23	4320	
	24	4319	4114
K_4	25	4241	
	26	4372	
	27	4326	
	28	4324	4117
Complete coupled-channels:			3470

dense distribution between 4.5 and 4.7 GeV, an enlarged part whose mass region is from 4.4 to 4.7 GeV is shown in the bottom panel of Fig. 4. Therein, the scattering nature of the radial excited states $\eta_c K$, ψK^* and DD_s is also well presented. One can realize that the obtained reso-

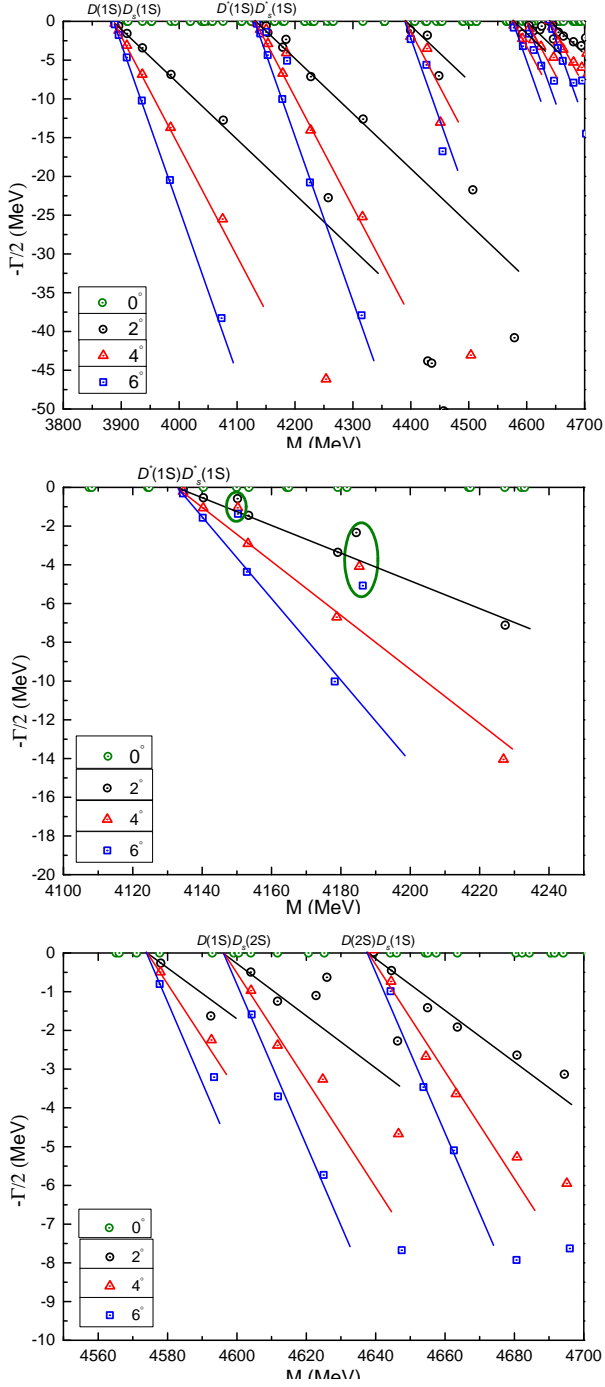


FIG. 3. *Top panel:* Complex energy spectrum of the $c\bar{c}s\bar{q}$ system with $J^P = 0^+$ from the coupled-channel calculation with CSM. Particularly, the $(c\bar{c})(s\bar{q})$ di-meson channels are excluded. The parameter θ varies from 0° to 6° . *Middle panel:* Enlarged top panel, with real values of energy ranging from 4.10 GeV to 4.25 GeV. *Bottom panel:* Enlarged top panel, with real values of energy ranging from 4.55 GeV to 4.70 GeV.

nance states in the coupled-channels investigations discussed above, $\eta_c(2S)K(1S)(4255)$, $\psi(2S)K^*(1S)(4675)$, $D^*(1S)D_s^*(1S)(4150)$, etc., turn to be scattering ones be-

TABLE VIII. The distance, in fm, between any two quarks of the $J^P = 0^+$ $c\bar{c}s\bar{q}$ tetraquark resonance state obtained in all exotic configurations' coupled-channels calculation. These resonances, which masses are below 4.3 GeV, are labeled in the first column.

State	$r_{c\bar{c}}$	$r_{c\bar{q}}$	$r_{\bar{c}s}$	$r_{c\bar{q}}$	r_{cs}	$r_{s\bar{q}}$
$Z_{cs}(3841)$	0.35	0.76	0.70	0.76	0.70	0.69
$Z_{cs}(4105)$	0.51	0.84	0.69	0.77	0.76	0.85
$Z_{cs}(4156)$	0.42	0.98	0.92	0.98	0.91	0.89
$Z_{cs}(4193)$	0.42	1.16	1.13	1.15	1.14	1.02
$Z_{cs}(4258)$	0.64	0.82	0.63	0.73	0.73	0.91

cause, in a complete coupled-channels calculation, these resonances easily decay to lower $(c\bar{c})(s\bar{q})$ or $(c\bar{q})(s\bar{c})$ di-meson scattering states.

B. The $J^P = 1^+$ $c\bar{c}s\bar{q}$ tetraquark system

The available 42 channels that include meson-meson, diquark-antidiquark and K-type structures are listed in Table V. The lowest-lying $c\bar{c}s\bar{q}$ tetraquark states with spin-parity $J^P = 1^+$ are firstly calculated within the real-range approximation and summarized in Table IX. Particularly, the allowed channels are listed in the 1st and 5th columns, when possible, the non-interacting meson-meson experimental threshold values are labeled in parentheses. The assigned indexes for the channels are shown in the 2nd and 6th columns. The theoretical mass obtained in each channel is shown in the 3rd and 7th columns, besides, the coupled result for each kind of configuration is presented in the 4th and last columns. The last row of Table IX indicates the lowest-lying mass of the system in a fully coupled-channels case. When the CSM is used in the coupled-channels calculations, Figs. 5 to 10 show the distribution of complex eigen-energies and, therein, the obtained resonance states are indicated inside circles. Furthermore, when a calculation which all channels listed in Table V are considered except the color-singlet di-meson cases is performed, the obtained resonances within a mass region 3.9~4.2 GeV, along with their inner structures, are summarized in Table X. Now let us discuss the details of $c\bar{c}s\bar{q}$ tetraquark in each three kind of investigations below.

Exotic states in $(c\bar{c})(s\bar{q})$ di-meson channels: There are six $(c\bar{c})(s\bar{q})$ di-meson channels contributing to the tetraquark system in 1^+ case, *i.e.*, $\eta_c K^*$, $J/\psi K$ and $J/\psi K^*$ states in color-singlet and -octet channels. From Table IX, we find that the three color-singlet channels are all unbound, the lowest-lying one, $J/\psi K$, is at 3578 MeV, the next one is $\eta_c K^*$ with mass at 3896 MeV, and $J/\psi K^*$ is at 4004 MeV. Their corresponding hidden-color channels masses are all ~ 4.4 GeV.

Additionally, a complex-range computation is performed in the coupled-channels study where the $(c\bar{c})(s\bar{q})$

TABLE IX. Lowest-lying $c\bar{c}s\bar{q}$ tetraquark states with $J^P = 1^+$ calculated within the real range formulation of the chiral quark model. The allowed meson-meson, diquark-antidiquark and K-type configurations are listed in the first and fifth columns; when possible, the experimental value of the non-interacting meson-meson threshold is labeled in parentheses. Each channel is assigned an index in the 2nd and 6th columns. The theoretical mass obtained in each channel is shown in the 3rd and 7th columns and the coupled result for each kind of configuration is presented in the 4th and last columns. When a complete coupled-channels calculation is performed, last row of the table indicates the lowest-lying mass. (unit: MeV).

Channel	Index	M	Mixed	Channel	Index	M	Mixed
$(\eta_c K^*)^1(3873)$	1	3896		K_1	19	4426	
$(J/\psi K)^1(3591)$	2	3578		K_1	20	4422	
$(J/\psi K^*)^1(3989)$	3	4004		K_1	21	4443	
$(DD_s^*)^1(3982)$	4	4012		K_1	22	4231	
$(D^* D_s)^1(3975)$	5	4006		K_1	23	4266	
$(D^* D_s^*)^1(4119)$	6	4132	3578	K_1	24	4188	4186
$(\eta_c K^*)^8$	7	4448		K_2	25	4215	
$(J/\psi K)^8$	8	4424		K_2	26	4252	
$(J/\psi K^*)^8$	9	4434		K_2	27	4175	
$(DD_s^*)^8$	10	4403		K_2	28	4420	
$(D^* D_s)^8$	11	4401		K_2	29	4427	
$(D^* D_s^*)^8$	12	4361	4224	K_2	30	4442	4168
$(cs)_3(\bar{c}\bar{q})_3^*$	13	4352		K_3	31	4283	
$(cs)_3^*(\bar{c}\bar{q})_3$	14	4357		K_3	32	4306	
$(cs)_3^*(\bar{c}\bar{q})_3^*$	15	4350		K_3	33	4340	
$(cs)_6(\bar{c}\bar{q})_6^*$	16	4342		K_3	34	4314	
$(cs)_6^*(\bar{c}\bar{q})_6$	17	4339		K_3	35	4348	
$(cs)_6^*(\bar{c}\bar{q})_6^*$	18	4270	4184	K_3	36	4349	4178
				K_4	37	4309	
				K_4	38	4319	
				K_4	39	4362	
				K_4	40	4327	
				K_4	41	4353	
				K_4	42	4349	4191
Complete coupled-channels:							3578

dimeson structures, diquark-antidiquark configurations and K-type ones are considered. Within a complex angle θ varied from 0° to 6° , Fig. 5 shows the distribution of calculated complex energy dots. In particular, the scattering states of $J/\psi K$, $\eta_c K^*$ and $J/\psi K^*$ are well presented in a mass region 3.5~4.7 GeV of the top panel of Fig. 5. However, there are three stable resonance poles, encircled by green lines, which can be identified as $\psi(2S)K(1S)$ molecular resonances. Their calculated masses and widths are, all in MeV, (4254, 0.8), (4267, 6.2) and (4303, 1.0). As one could conclude, the $Z_{cs}(4220)$ would be explained, too, as a $\psi(2S)K(1S)(4254)$ resonance in 1^+ state.

Meanwhile, since there is a dense distribution of complex energies at around 4.6 GeV, an enlarged panel whose mass range goes from 4.5 to 4.7 GeV is shown at the

bottom of Fig. 5. Therein, the radial excitation states of $\eta_c K^*$ and $J/\psi K^{(*)}$ are clearly presented and no resonance pole is obtained.

Exotic states in $(c\bar{q})(s\bar{c})$ dimeson channels: One can find in Table IX that there are six $(c\bar{q})(s\bar{c})$ dimeson channels which contribute to the tetraquark system with 1^+ quantum numbers, *i.e.*, DD_s^* , D^*D_s and $D^*D_s^*$ states in color-singlet and -octet channels. Within the real-range single channel approach, their theoretical masses in color-singlet channels are ~ 4.0 GeV, except for $D^*D_s^*$ at 4132 MeV. The hidden-color channels masses are higher and generally lie at around 4.4 GeV. Although these values are quite close to the experimental data of $Z_{cs}(4000)$, the scattering nature of $D^{(*)}D_s^{(*)}$ channel remains.

The coupled-channels result by CSM is shown in Fig. 6, within a mass range from 4.0 to 4.7 GeV. The scatter-

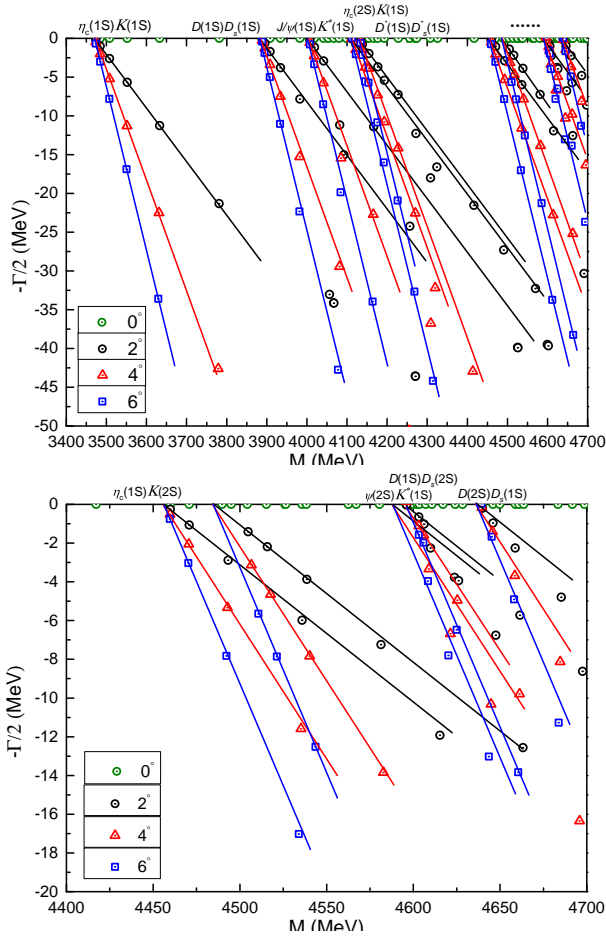


FIG. 4. *Top panel:* The complete coupled-channels calculation of the $c\bar{c}s\bar{q}$ tetraquark system with $J^P = 0^+$ quantum numbers. We use the complex-scaling method of the chiral quark model varying θ from 0° to 6° . *Bottom panel:* Enlarged top panel, with real values of energy ranging from 4.40 GeV to 4.70 GeV.

ing nature of DD_s^* and D^*D_s is clearly demonstrated. Nevertheless, two narrow $D^*(1S)D_s^*(1S)$ resonances are obtained and circled in green. The calculated masses and widths are (4254, 1.6) MeV and (4594, 0.6) MeV, respectively. Accordingly, there is a degeneration between the $D^*(1S)D_s^*(1S)$ and $\psi(2S)K(1S)$ channels at 4254 MeV.

The fully coupled-channels case: Apart from the 12 meson-meson channels listed in Table IX, the single channel calculation for diquark-antidiquark structures and K-type ones is also analyzed. In particular, there are six channels in each kind of configurations, the diquark-antidiquark channels are ~ 4.3 GeV, and the K-type ones are lying from 4.2 to 4.4 GeV. In addition, when a coupled-channels study is done in each configuration, the lowest mass, 3578 MeV, is still equal to the theoretical threshold value of $J/\psi K$. The mass of the hidden-color coupled-channels result is higher and at 4224 MeV. Meanwhile, the diquark-antidiquark and K-type structures coupled masses are all around 4.18 GeV.

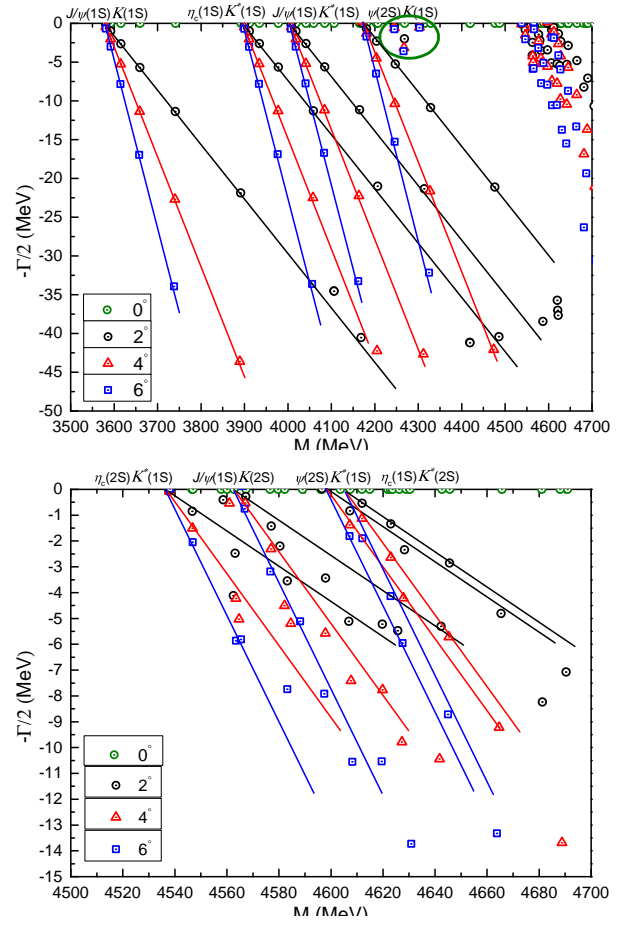


FIG. 5. *Top panel:* The coupled-channels calculation of the $c\bar{c}s\bar{q}$ tetraquark system with $J^P = 1^+$ quantum numbers. Particularly, the $(c\bar{q})(s\bar{c})$ dimeson channels are excluded. We use the complex-scaling method of the chiral quark model varying θ from 0° to 6° . *Bottom panel:* Enlarged top panel, with real values of energy ranging from 4.50 GeV to 4.70 GeV.

TABLE X. The distance, in fm, between any two quarks of the $J^P = 1^+$ $c\bar{c}s\bar{q}$ tetraquark resonance state obtained in all exotic configurations' coupled-channels calculation. These resonances, which masses are around 3.9~4.2 GeV, are labeled in the first column.

State	$r_{\bar{c}c}$	$r_{\bar{c}\bar{q}}$	$r_{\bar{c}s}$	$r_{c\bar{q}}$	r_{cs}	$r_{s\bar{q}}$
$Z_{cs}(3947)$	0.41	0.78	0.71	0.77	0.71	0.70
$Z_{cs}(4038)$	0.35	0.95	0.87	0.95	0.87	0.87
$Z_{cs}(4137)$	0.44	0.94	0.83	0.92	0.86	0.88
$Z_{cs}(4199)$	0.58	0.80	0.67	0.74	0.73	0.87
$Z_{cs}(4211)$	0.60	0.84	0.65	0.76	0.75	0.90

However, no bound state is found in 1^+ state when a complete coupled-channels calculation is studied and the lowest mass remains at 3578 MeV.

In order to have a much more detailed investigation on the strange hidden-charm tetraquark in 1^+ state,

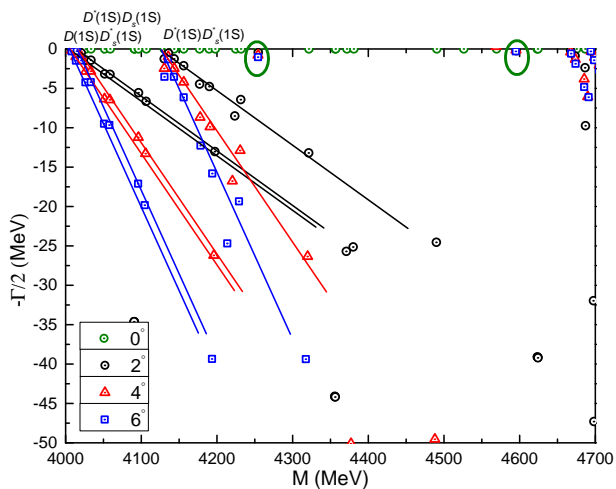


FIG. 6. The coupled-channels calculation of the $c\bar{c}s\bar{q}$ tetraquark system with $J^P = 1^+$ quantum numbers. Particularly, the $(c\bar{c})(s\bar{q})$ dimeson channels are excluded. We use the complex-scaling method of the chiral quark model varying θ from 0° to 6° .

a coupled-channels computation of all exotic structures where only the dimeson structures in color-singlet channels are excluded is performed. Table X summarizes the Z_{cs} resonances within 3.9~4.2 GeV. The five exotic states are compact structures and the calculated distances between any two (anti)quark and quark-antiquark are less than 1.0 fm. Particularly, the two lower states, $Z_{cs}(3947)$ and $Z_{cs}(4038)$, are well compatible with the recently reported exotic structures [1, 2]. Hence, the $Z_{cs}(3985)$ and $Z_{cs}(4000)$ should be considered as $J^P = 1^+$ $c\bar{c}s\bar{q}$ tetraquark with a large compact component.

Last but not least, a fully coupled-channels calculation in CSM is investigated and the result is listed in Fig. 10. Firstly, within a mass region 3.5~4.7 GeV, the scattering states of $J/\psi K^{(*)}$, $\eta_c K^*$ and $D^{(*)}D_s^*$ are clearly shown in the top panel of Fig. 10. One could see that with the rotated angle θ varied from 0° to 6° , the calculated complex energy dots always descend and basically align along the corresponding threshold lines. However, since there are dense distributions at around 4.1 and 4.6 GeV, enlarged parts on these two energy regions are presented in, respectively, the middle and bottom panels of Fig. 10. No resonance pole is obtained in the energy range 4.0~4.3 GeV of the middle panel; however, one narrow resonance is found at higher energy, shown in the bottom panel. With a mass range from 4.5 to 4.7 GeV, four continuum (scattering) states of $\eta_c K^*$, $J/\psi K$ and DD_s^* in radial excitations are well shown; meanwhile, a fixed pole is circled at (4695, 1.3) MeV. Accordingly, the $X(4685)$ state with 1^+ quantum numbers reported by the LHCb collaboration [2] could be explained as a $D(1S)D_s^*(2S)(4695)$ resonance.

It is worth emphasizing herein that the resonances obtained in the different kinds of coupled-channels investigations are quite unstable and they easily decay

TABLE XI. Lowest-lying $c\bar{c}s\bar{q}$ tetraquark states with $J^P = 2^+$ calculated within the real range formulation of the chiral quark model. The allowed meson-meson, diquark-antidiquark and K-type configurations are listed in the first column; when possible, the experimental value of the non-interacting meson-meson threshold is labeled in parentheses. Each channel is assigned an index in the 2nd column. The theoretical mass obtained in each channel is shown in the 3rd column and the coupled result for each kind of configuration is presented in the last column. When a complete coupled-channels calculation is performed, last row of the table indicates the lowest-lying mass. (unit: MeV).

Channel	Index	M	Mixed
$(J/\psi K^*)^1(3989)$	1	4004	
$(D^* D_s^*)^1(4119)$	2	4132	4004
$(J/\psi K^*)^8$	3	4466	
$(D^* D_s^*)^8$	4	4411	4317
$(cs)_3^*(\bar{c}\bar{q})_3^*$	5	4381	
$(cs)_6^*(\bar{c}\bar{q})_6^*$	6	4346	4296
K_1	7	4462	
	8	4296	4296
K_2	9	4283	
	10	4461	4283
K_3	11	4348	
	12	4373	4302
K_4	13	4367	
	14	4378	4302
Complete coupled-channels:			4004

to a meson-meson scattering state, *e.g.*, the $Z_{cs}(3947)$, $Z_{cs}(4038)$ and $Z_{cs}(4137)$, which are obtained in a coupled-channels calculation with only exotic color structures are unavailable in the complete coupled-channels case of Fig. 10.

C. The $J^P = 2^+$ $c\bar{c}s\bar{q}$ tetraquark system

Table VI lists the allowed 14 channels in the highest spin state of the $c\bar{c}s\bar{q}$ tetraquark system considered herein. Particularly, there are four meson-meson structures, two diquark-antidiquark structures and 8 K-type ones. In a real-range investigation, Table XI summarizes the calculated results of these channels. Therein, the physical channels are listed in the first column, and they are indexed in the following one. The theoretical mass of each channel and coupled result in each kind of configuration is listed in the 3rd and 4th column, respectively. Meanwhile, the lowest-lying mass of system in a complete

coupled-channels is listed in the last row of Table XI. Additionally, Figs. 7 to 9 show the coupled-channels results in a complex-range study, and the resonance states are indicated inside circles. When coupling is only considered for the exotic color configurations: the hidden-color channels of dimeson structures, diquark-antidiquark structures and K-type ones, Table XII presents the exotic resonances whose masses are less than 4.3 GeV, and their inner structures are also analyzed. Further details are discussed in the following.

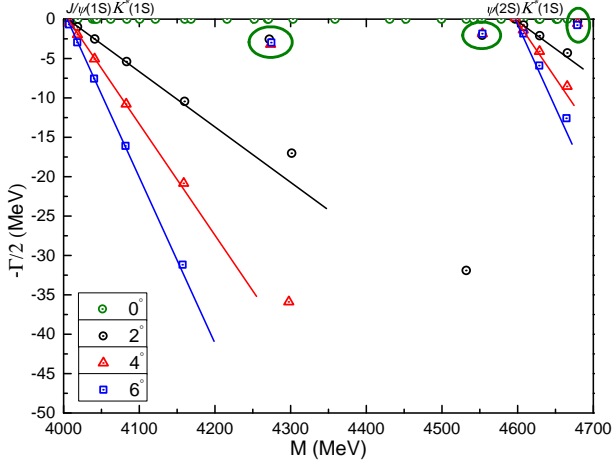


FIG. 7. The coupled-channels calculation of the $c\bar{c}s\bar{q}$ tetraquark system with $J^P = 2^+$ quantum numbers. Particularly, the $(c\bar{q})(s\bar{c})$ dimeson channels are excluded. We use the complex-scaling method of the chiral quark model varying θ from 0° to 6° .

Exotic states in $(c\bar{c})(s\bar{q})$ dimeson channels: The calculated theoretical masses for the $J/\psi K^*$ in both color-singlet and -octet channels are 4004 and 4466 MeV, respectively (see Table XI). Therefore, the $(J/\psi K^*)^1$ state is of scattering nature and cannot be identified as the $Z_{cs}(4000)$ reported by the LHCb collaboration.

Figure 7 illustrates the distribution of complex energies when a coupled-channels investigation that includes the $J/\psi K^*$ dimeson, diquark-antidiquark and K-type structures is performed in the CSM. Within a mass region 4.0~4.7 GeV, the scattering states of $J/\psi(1S)K^*(1S)$ and $\psi(2S)K^*(1S)$ are well obtained. However, one could also realize that three narrow resonances, circled with green lines, are not sensitive with respect to the variation of the complex angle θ . The calculated masses and widths for these resonances are (4271, 5.2) MeV, (4553, 4.0) MeV and (4678, 1.6) MeV. In analogy with the $\psi(2S)K^*(1S)(4675)$ resonance obtained in the 0^+ channel, the $\psi(2S)K^*(1S)(4678)$ resonance obtained here could also be related to the announced $X(4630)$, since the spin-parity of the $X(4685)$ state has been experimentally assigned to be 1^+ .

Exotic states in $(c\bar{q})(s\bar{c})$ dimeson channels: Considering the $D^*D_s^*$ di-meson channel with quantum numbers 2^+ shown in Table XI, the lowest masses of color-

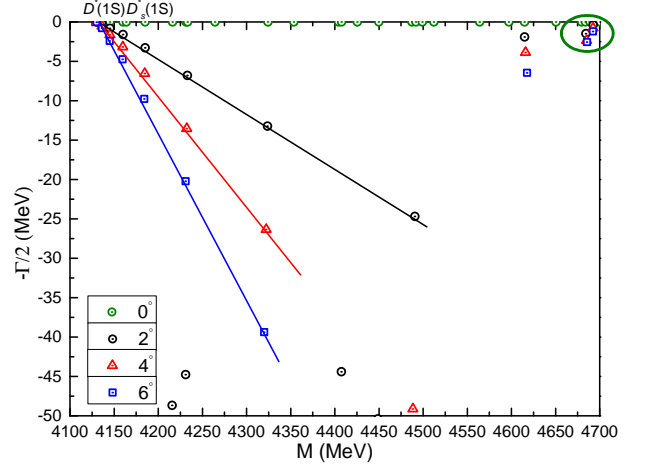


FIG. 8. The coupled-channels calculation of the $c\bar{c}s\bar{q}$ tetraquark system with $J^P = 2^+$ quantum numbers. Particularly, the $(c\bar{c})(s\bar{q})$ dimeson channels are excluded. We use the complex-scaling method of the chiral quark model varying θ from 0° to 6° .

TABLE XII. The distance, in fm, between any two quarks of the $J^P = 2^+$ $c\bar{c}s\bar{q}$ tetraquark resonance state obtained in all exotic configurations' coupled-channels calculation. These resonances, which masses are below 4.3 GeV, are labeled in the first column.

State	$r_{\bar{c}c}$	$r_{\bar{c}\bar{q}}$	$r_{\bar{c}s}$	$r_{c\bar{q}}$	r_{cs}	$r_{s\bar{q}}$
$Z_{cs}(4145)$	0.41	0.96	0.88	0.95	0.88	0.88
$Z_{cs}(4276)$	0.65	0.83	0.63	0.74	0.74	0.92

singlet and hidden-color structures are 4132 and 4411 MeV, respectively, and thus our conclusion on having scattering states in color-singlet channel remains. Figure 8 shows the distribution of the complex energy dots obtained in a coupled-channels calculation with $D^*D_s^*$ di-meson configurations, diquark-antidiquark structures and K-type arrangements. Particularly, the scattering nature of $D^*(1S)D_s^*(1S)$ is clearly shown in the 4.1~4.7 energy region. However, two quite close resonance poles are circled in the complex plane of Fig. 8. Therein, the two resonance states can be identified as $D^*(1S)D_s^*(1S)(4685)$ and $D^*(1S)D_s^*(1S)(4692)$, their widths are 4.8 and 1.6 MeV, respectively. Although the mass of the $D^*(1S)D_s^*(1S)(4685)$ structure extremely coincides with that of the $X(4685)$ state, the spin-parity 2^+ is different from its experimental assignment.

The fully coupled-channels case: As shown in Table XI, the exotic configurations, which are diquark-antidiquark and K-type arrangements, lie generally in the mass range 4.3~4.4 GeV. In coupled-channels computations for each kind of configuration, the lowest-lying mass located at 4004 MeV is still the theoretical value of the $(J/\psi K^*)^1$ threshold channel, and this fact is not changed in a fully coupled-channels calculation. Meanwhile, the

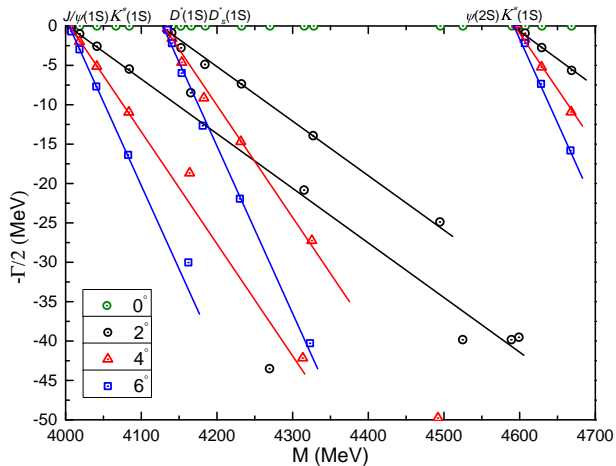


FIG. 9. The complete coupled-channels calculation of the $c\bar{c}s\bar{q}$ tetraquark system with $J^P = 2^+$ quantum numbers. We use the complex-scaling method of the chiral quark model varying θ from 0° to 6° .

other coupled-channels structures have higher masses at around 4.3 GeV.

When all of the exotic color structures are considered in a coupled-channels study, Table XII lists two resonance states whose mass is below 4.3 GeV. The distances between any two quarks are less than 1 fm, and hence they are good candidates of compact tetraquarks with color resonance structures.

In a further step, when the CSM is employed in a fully coupled-channels calculation, Fig. 9 shows the distribution of the scattering states for $J/\psi(1S)K^*(1S)$, $D^*(1S)D_s^*(1S)$ and $\psi(2S)K^*(1S)$ in the mass region 4.0~4.7 GeV. As in the case of spin-parity 0^+ , no bound state is found and the calculated resonance states in different kinds of coupled-channels studies, e.g., $\psi(2S)K^*(1S)$ (4678), $D^*(1S)D_s^*(1S)$ (4685) and $D^*(1S)D_s^*(1S)$ (4692), etc., are quite unstable decaying easily to the $J/\psi K^*$ and $D^*D_s^*$ meson-meson scattering states.

IV. SUMMARY

A systematical investigation of hidden-charm tetraquarks with strange content: $c\bar{c}s\bar{q}$ ($q = u, d$), has been performed within a chiral quark model formalism. The model, which includes the one-gluon exchange, a linear-screened confining and Goldstone-

boson exchange interactions between quarks, has been successfully applied to the description of hadron, hadron-hadron and multi-quark phenomenology. In particular, the hidden-charm pentaquarks and doubly charmed tetraquark are well predicted in our previous theoretical investigations. Our formulation in real- and complex-scaling method of the theoretical formalism allows us to distinguish three kinds of scattering singularities: bound, resonance and scattering. Furthermore, the meson-meson, diquark-antidiquark and K-type configurations, plus their couplings, are considered for the tetraquark system. Finally, the Rayleigh-Ritz variational method is employed in dealing with the spatial wave functions of the $c\bar{c}s\bar{q}$ tetraquark states, which are expanded by means of the well-known Gaussian expansion method (GEM) of Ref. [56].

Our theoretical findings can be summarized as follows.

- The Z_{cs} (3985) and Z_{cs} (4000) can both be identified as compact $c\bar{c}s\bar{q}$ tetraquark states with $J^P = 1^+$, and their sizes are less than 1 fm.
- The Z_{cs} (4220) is compatible with being a hadronic molecular resonance of either $\eta_c(2S)K(1S)$ (4255) with spin-parity 0^+ or $\psi(2S)K(1S)$ (4254) and $D^*(1S)D_s^*(1S)$ (4254) with 1^+ quantum numbers.
- The X (4685) can be well identified as a hadronic molecular resonance whose structure resembles the $D(1S)D_s^*(2S)$ (4695) arrangement with quantum numbers $J^P = 1^+$.
- An extra exotic state Z_{cs} (4150), which is predicted in other theoretical investigation, can be explained as $D^*(1S)D_s^*(1S)$ resonance in 0^+ state herein.
- Several compact $c\bar{c}s\bar{q}$ tetraquark resonances within a mass region 3.8~4.2 GeV and narrow hadronic molecular resonances, which locate at 4.1~4.3 GeV and 4.5~4.6 GeV, are obtained in 0^+ , 1^+ and 2^+ states, respectively.

ACKNOWLEDGMENTS

Work partially financed by: National Natural Science Foundation of China under Grant Nos. 11535005 and 11775118; the Ministerio Español de Ciencia e Innovación, grant no. PID2019-107844GB-C22; and Junta de Andalucía under contract no. Operativo FEDER Andalucía 2014-2020 UHU-1264517, P18-FR-5057 and PAIDI FQM-370.

[1] M. Ablikim *et al.* (BESIII), Phys. Rev. Lett. **126**, 102001 (2021), arXiv:2011.07855 [hep-ex].
 [2] R. Aaij *et al.* (LHCb), (2021), arXiv:2103.01803 [hep-ex].
 [3] Z. Yang, X. Cao, F.-K. Guo, J. Nieves, and

M. P. Valderrama, Phys. Rev. D **103**, 074029 (2021), arXiv:2011.08725 [hep-ph].
 [4] L. Meng, B. Wang, and S.-L. Zhu, Phys. Rev. D **102**, 111502 (2020), arXiv:2011.08656 [hep-ph].

- [5] Z.-F. Sun and C.-W. Xiao, (2020), arXiv:2011.09404 [hep-ph].
- [6] B. Wang, L. Meng, and S.-L. Zhu, Phys. Rev. D **103**, L021501 (2021), arXiv:2011.10922 [hep-ph].
- [7] N. Ikeno, R. Molina, and E. Oset, Phys. Lett. B **814**, 136120 (2021), arXiv:2011.13425 [hep-ph].
- [8] Z.-M. Ding, H.-Y. Jiang, D. Song, and J. He, (2021), arXiv:2107.00855 [hep-ph].
- [9] Q.-N. Wang, W. Chen, and H.-X. Chen, (2020), arXiv:2011.10495 [hep-ph].
- [10] Y.-J. Xu, Y.-L. Liu, C.-Y. Cui, and M.-Q. Huang, (2020), arXiv:2011.14313 [hep-ph].
- [11] M.-J. Yan, F.-Z. Peng, M. Sánchez Sánchez, and M. Pavon Valderrama, (2021), arXiv:2102.13058 [hep-ph].
- [12] Z.-H. Guo and J. A. Oller, Phys. Rev. D **103**, 054021 (2021), arXiv:2012.11904 [hep-ph].
- [13] R. Chen and Q. Huang, Phys. Rev. D **103**, 034008 (2021), arXiv:2011.09156 [hep-ph].
- [14] M.-Z. Liu, J.-X. Lu, T.-W. Wu, J.-J. Xie, and L.-S. Geng, (2020), arXiv:2011.08720 [hep-ph].
- [15] X. Jin, X. Liu, Y. Xue, H. Huang, and J. Ping, (2020), arXiv:2011.12230 [hep-ph].
- [16] M. Karliner and J. L. Rosner, (2021), arXiv:2107.04915 [hep-ph].
- [17] B.-D. Wan and C.-F. Qiao, Nucl. Phys. B **968**, 115450 (2021), arXiv:2011.08747 [hep-ph].
- [18] Z.-G. Wang, Chin. Phys. C **45**, 073107 (2021), arXiv:2011.10959 [hep-ph].
- [19] J.-Z. Wang, Q.-S. Zhou, X. Liu, and T. Matsuki, Eur. Phys. J. C **81**, 51 (2021), arXiv:2011.08628 [hep-ph].
- [20] M.-C. Du, Q. Wang, and Q. Zhao, (2020), arXiv:2011.09225 [hep-ph].
- [21] X. Cao, J.-P. Dai, and Z. Yang, Eur. Phys. J. C **81**, 184 (2021), arXiv:2011.09244 [hep-ph].
- [22] K. Azizi and N. Er, Eur. Phys. J. C **81**, 61 (2021), arXiv:2011.11488 [hep-ph].
- [23] J. Y. Süngü, A. Türkan, H. Sundu, and E. V. Veliev, (2020), arXiv:2011.13013 [hep-ph].
- [24] H.-X. Chen, (2021), arXiv:2103.08586 [hep-ph].
- [25] L. Meng, B. Wang, G.-J. Wang, and S.-L. Zhu, (2021), 10.1016/j.scib.2021.06.026, arXiv:2104.08469 [hep-ph].
- [26] X.-D. Yang, F.-L. Wang, Z.-W. Liu, and X. Liu, (2021), arXiv:2103.03127 [hep-ph].
- [27] Z.-G. Wang, (2021), arXiv:2103.04236 [hep-ph].
- [28] X. Chen, Y. Tan, and Y. Chen, Phys. Rev. D **104**, 014017 (2021), arXiv:2103.07347 [hep-ph].
- [29] J. F. Giron, R. F. Lebed, and S. R. Martinez, (2021), arXiv:2106.05883 [hep-ph].
- [30] A. Türkan, J. Y. Süngü, and E. V. Veliev, (2021), arXiv:2103.05515 [hep-ph].
- [31] Y.-H. Ge, X.-H. Liu, and H.-W. Ke, (2021), arXiv:2103.05282 [hep-ph].
- [32] U. Ozdem and A. K. Yildirim, (2021), arXiv:2104.13074 [hep-ph].
- [33] G. Yang, J. Ping, and F. Wang, Phys. Rev. **D95**, 014010 (2017).
- [34] G. Yang, J. Ping, and J. Segovia, Phys. Rev. D **99**, 014035 (2019), arXiv:1809.06193 [hep-ph].
- [35] G. Yang, J. L. Ping, and J. Segovia, Phys. Rev. D **101**, 074030 (2020).
- [36] G. Yang, J. L. Ping, and J. Segovia, Phys. Rev. D **101**, 014001 (2020).
- [37] G. Yang, J. Ping, and J. Segovia, Phys. Rev. D **102**, 054023 (2020).
- [38] G. Yang, J. Ping, and J. Segovia, Phys. Rev. D **103**, 074011 (2021), arXiv:2101.04933 [hep-ph].
- [39] R. Aaij *et al.* (LHCb), Phys. Rev. Lett. **115**, 072001 (2015).
- [40] R. Aaij *et al.* (LHCb), Phys. Rev. Lett. **122**, 222001 (2019).
- [41] R. Aaij *et al.* (LHCb), (2021), arXiv:2109.01038 [hep-ex].
- [42] R. Aaij *et al.* (LHCb), (2021), arXiv:2109.01056 [hep-ex].
- [43] J. Segovia, A. M. Yasser, D. R. Entem, and F. Fernandez, Phys. Rev. **D78**, 114033 (2008).
- [44] J. Segovia, D. R. Entem, F. Fernandez, and E. Hernandez, Int. J. Mod. Phys. E **22**, 1330026 (2013), arXiv:1309.6926 [hep-ph].
- [45] J. Segovia, P. G. Ortega, D. R. Entem, and F. Fernández, Phys. Rev. D **93**, 074027 (2016), arXiv:1601.05093 [hep-ph].
- [46] G. Yang, J. Ping, P. G. Ortega, and J. Segovia, Chin. Phys. C **44**, 023102 (2020), arXiv:1904.10166 [hep-ph].
- [47] J. Segovia, A. M. Yasser, D. R. Entem, and F. Fernandez, Phys. Rev. D **80**, 054017 (2009).
- [48] J. Segovia, D. Entem, and F. Fernandez, Phys. Rev. D **83**, 114018 (2011).
- [49] J. Segovia, D. R. Entem, and F. Fernández, Phys. Lett. B **715**, 322 (2012), arXiv:1205.2215 [hep-ph].
- [50] J. Segovia, D. R. Entem, and F. Fernandez, Phys. Rev. D **91**, 094020 (2015), arXiv:1502.03827 [hep-ph].
- [51] P. G. Ortega, J. Segovia, D. R. Entem, and F. Fernandez, Phys. Rev. D **81**, 054023 (2010), arXiv:0907.3997 [hep-ph].
- [52] P. G. Ortega, J. Segovia, D. R. Entem, and F. Fernandez, Phys. Rev. D **94**, 074037 (2016), arXiv:1603.07000 [hep-ph].
- [53] P. G. Ortega, J. Segovia, D. R. Entem, and F. Fernández, Phys. Rev. D **95**, 034010 (2017), arXiv:1612.04826 [hep-ph].
- [54] P. G. Ortega, J. Segovia, D. R. Entem, and F. Fernandez, Eur. Phys. J. C **80**, 223 (2020), arXiv:2001.08093 [hep-ph].
- [55] G. Yang, J. Ping, and J. Segovia, Sym. **12**, 1869 (2020).
- [56] E. Hiyama, Y. Kino, and M. Kamimura, Prog. Part. Nucl. Phys. **51**, 223 (2003).
- [57] J. Aguilar and J. M. Combes, Commun. Math. Phys. **22**, 269 (1971).
- [58] E. Balslev and J. M. Combes, Commun. Math. Phys. **22**, 280 (1971).
- [59] J. Vijande, F. Fernandez, and A. Valcarce, J. Phys. **G31**, 481 (2005), arXiv:hep-ph/0411299 [hep-ph].
- [60] M. D. Scadron, Phys. Rev. **D26**, 239 (1982).
- [61] G. S. Bali, H. Neff, T. Duessel, T. Lippert, and K. Schilling (SESAM), Phys. Rev. **D71**, 114513 (2005), arXiv:hep-lat/0505012 [hep-lat].
- [62] J. Segovia, D. R. Entem, and F. Fernandez, Phys. Lett. **B662**, 33 (2008).

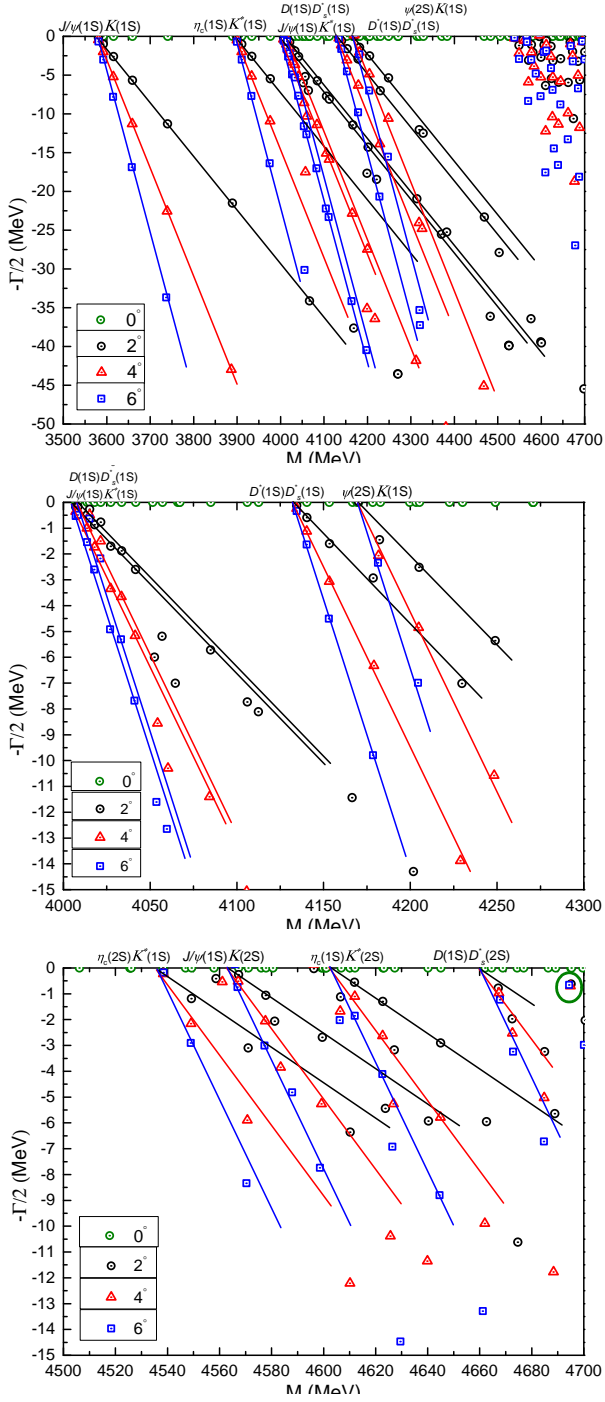


FIG. 10. *Top panel:* The complete coupled-channels calculation of the $c\bar{c}s\bar{q}$ tetraquark system with $J^P = 1^+$ quantum numbers. We use the complex-scaling method of the chiral quark model varying θ from 0° to 6° . *Middle panel:* Enlarged top panel, with real values of energy ranging from 4.00 GeV to 4.30 GeV. *Bottom panel:* Enlarged top panel, with real values of energy ranging from 4.50 GeV to 4.70 GeV.